

An Inline Quarter-Mode SIW Bandpass Filter Based on Frequency-Dependent Coupling Structures with Controllable Transmission Zeros

Zhiwei Shi, Guohui Li*, Yulu Song, and Binbin Cheng

Abstract—An inline quarter-mode substrate integrated waveguide (QMSIW) filter with controllable finite transmission zeros (FTZs) is presented based on a novel frequency-dependent coupling structure, which is constructed by a microstrip line with a pair of symmetric metallized via/buried holes and a magnetic coupling iris between two resonant cavities. FTZ can be independently introduced and controlled on both sides of passband to achieve high selectivity while keeping the filter compact configuration unchanged. For demonstration, the proposed structure is analyzed in detail. An inline fourth-order QMSIW bandpass filter (BPF) with two upper FTZs is designed, fabricated, and measured. The synthesis results, EM results, and measured results are in accordance with each other, which confirms the effectiveness of the proposed method.

1. INTRODUCTION

With the increasing development of modern wireless communication techniques, filters as fundamental components for numerous wireless products or communication systems need to have some characteristics, for example, compact size, better out-of-band rejection, easy integration with other components, and low manufacturing costs. Utilizing finite transmission zeros (TZs) is crucial in modern microwave filter design to improve out-of-band frequency selectivity. Besides cross-coupling and non-resonating node (NRN), frequency-dependent coupling (FDC) is the third method of introducing additional transmission zeros (TZs) [1–11] to achieve sharp cut-off performance [4] and wideband filters [12]. TZs can be generated and independently controlled without any cross-coupled or extracted-pole structures. FDC allows one to generate multiple TZs in an in-line topology without increasing the filter order, dimensions, and coupling paths. This allows for higher selectivity and better rejection while taking advantage of the high isolation of inline topology [1, 2, 4, 6, 7, 11].

Inline filters with FDC can generate multiple transmission zeros, and each TZ can be individually controlled. Considering capacitance and coupling matrix (CM) together [13], a matrix transformation procedure is presented to synthesize inline topology filters with FDCs [1]. Based on an iterative method, a high selectivity filtering response in which there are $N-1$ independently controllable TZs for an N th-order inline topology was proposed in [2]. In general, FDC is practically implemented by grounded coplanar waveguides [3–5, 7] and meander lines with via holes [8]. It can also be realized through a shorted stub with an additional septum between cavities [6], but this increases the size of the filter. Besides single layer printed circuit boards (PCB), a two-layer PCB can also be utilized to design quasi-elliptic filters with FDC [7]. In particular, some filters with FDC structures based on substrate integrated waveguide (SIW) technology are proposed [3–8]. SIW can be well integrated with other circuits due to its planar characteristics. The field distribution in the SIW cavity is symmetrical at TE₁₀₁ mode,

Received 18 February 2021, Accepted 14 April 2021, Scheduled 22 April 2021

* Corresponding author: Guohui Li (ghlee@sohu.com).

The authors are with the Key Laboratory of Specialty Fiber Optics and Optical Access Network, Shanghai University, China.

and segmentation along with equivalent magnetic walls has no effect on its symmetry while preserving the field distribution, thus, symmetrical cutting can reduce circuit dimension. Quarter-mode substrate integrated waveguide (QMSIW) [14–17] combined with single-layer filters is proposed, which reduces the occupied area to one quarter. As shown in [18], the sizes of several eighth-mode substrate integrated waveguide (EMSIW) cavities including single and multi-layer board are only one-eighth of a conventional SIW resonant cavity.

In this paper, a novel FDC structure between two cavities based on a QMSIW is proposed, and the structure is implemented by magnetic coupling iris and a microstrip line with a pair of symmetric metallized holes. The metallized holes are located on both ends of microstrip line where the electric field is the strongest. It was found that the length of microstrip line and the depth of metallized holes mainly control the position of FTZ. Section 2 describes the details of the proposed configuration and the analysis of its implementation to realize the arbitrary position of FTZ in a second-order filter. Section 3 presents an inline QMSIW BPF with proposed structure, and a comparison of simulated and measured results to verify the method. Finally, Section 4 concludes the paper.

2. ANALYSIS OF PROPOSED FDC STRUCTURE

2.1. Structure of FDC

As shown in Fig. 1, the electric field distribution is symmetrical in a rectangle SIW cavity. The QMSIW can be obtained by bisecting the SIW cavity along with two fictitious magnetic walls, while preserving the field distribution of the original SIW cavity. From the evolution of QMSIW, it is apparent that QMSIW offers a new concept to design compact filters. The second-order QMSIW filter layout with the proposed FDC structure and resonators arrangement is shown in Fig. 2, where the direct coupling between two resonators is strongly frequency-independent. For this application, the FDC structure placed along one open side between two quarter-mode cavities is employed, where the metallized holes at the ends of microstrip line are located in the strongest electric field. The diameters of metallized holes are marked as d_f and depth as h_f . The gap between the left and right sides of the microstrip line is g_1 , while the gap below the line is g_2 . The capacitive part of the couplings is contributed by a microstrip line with length of f_y and width of f_x . This structure is employed to control the electric coupling strength. The electric field propagates along the microstrip line, which leads to electric coupling between two resonators. Two metallized holes are respectively loaded on the ends of microstrip line, which are close to the position of the strongest electric field in the cavity. So, it makes the microstrip line fully coupled with the cavity through the electric field. In addition, the inductive coupling is mainly controlled through the iris size g_3 . Thus, an FDC is caused by a composition of the capacitive and inductive parts of a field being propagated within a certain discontinuity, resulting in a mixed coupling. In consequence, a specific frequency-variant coupling can thus be approximately realized by properly selecting the combination of length f_y , width f_x , and g_3 in a mixed-coupled structure.

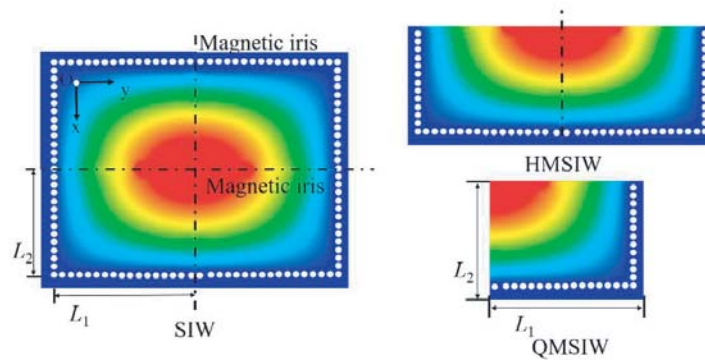


Figure 1. Electric field distribution of SIW, HMSIW, QMSIW.

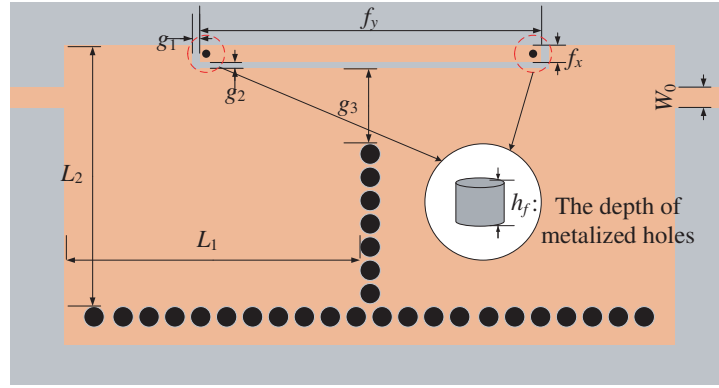


Figure 2. Layout of second-order filter with the proposed FDC structure.

2.2. Characteristic of the Proposed FDC Structure

The coupling coefficient K is calculated using the following formula (1), where f_1 and f_2 are the resonant frequencies of the coupled pair. Considering the FDC, admittance matrix can be derived as Eq. (2), where FDC matrix and coupling matrix are denoted by C and M . The de-normalized admittance inverter of FDC bandpass filter is given by Eq. (3). It can be observed that a lowpass prototype whose coupling coefficients are linear functions of the normalized frequency can be transformed into a constant coupling coefficients network. In practice, we need to look for a physical coupling structure to ensure that J_{ij} turns into zero at a particular frequency f_{tz} by considering only a small range around the centre frequency f_0 . It means that FDC can be achieved by means of a suitable mix of electrical and magnetic couplings and resonates at f_{tz} in the actual circuit design. Simultaneously, the coupling coefficient J_{ij} at centre frequency satisfies Equation (4). It is uncomplicated to find that the position of transmission zero is just the same as f_{tz} .

$$K = \pm \frac{f_2^2 - f_1^2}{f_2^2 + f_1^2} \tag{1}$$

$$A = -jG + \Omega C + M \tag{2}$$

$$J_{ij} = \frac{BW}{f_0} M_{ij} + C_{ij} \left(\frac{f}{f_0} - \frac{f_0}{f} \right) \tag{3}$$

$$J_{ij}|_{f_0} = \frac{BW}{f_0} M_{ij} \tag{4}$$

Considering weak coupling, in the case, the feed lines are placed where the electric field is weak and magnetic field is strong. From Figs. 3–4, the location of FTZs can be easily controlled by changing parameters h_f and f_y . To explain the design more precisely, the simulated S parameters and coupling coefficient versus different values of h_f and f_y are illustrated in Fig. 5. As shown in Fig. 3, the FTZ moves from the lower to the upper stopband while changing the depth of metallized hole h_f and keeping the other parameters constant, and the resonant frequencies remain constant. It can be observed from Fig. 4 that the FTZ is further away from the cut-off frequency with the decrease of f_y . Spurious frequency will be introduced due to the parasitic inductance resulting from the metal holes which are located at both ends of the structure and will move as f_y increases. The spurious frequency should be kept far away from the passband to avoid the influence on the filter design. However, FTZ may also be shifted away, which worsens the selectivity of the filter. Thus, care must be taken when the position of metal holes is adjusted. As for magnetic iris, it mainly controls the amplitude of magnetic coupling, whose size also has effect on the position of FTZ. Fig. 5 shows coupling coefficient of the proposed FDC structure with different parameters f_y and g_3 . It is apparent that the slope of electric coupling increases with the length of f_y , which means that electric coupling is dominant in mixed coupling. When different curves of inductive iris are compared, the slope of magnetic coupling increases with the width.

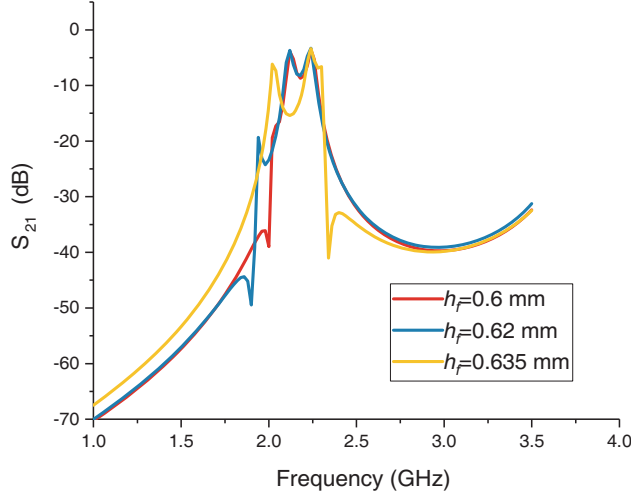


Figure 3. Simulated results versus different h_f .

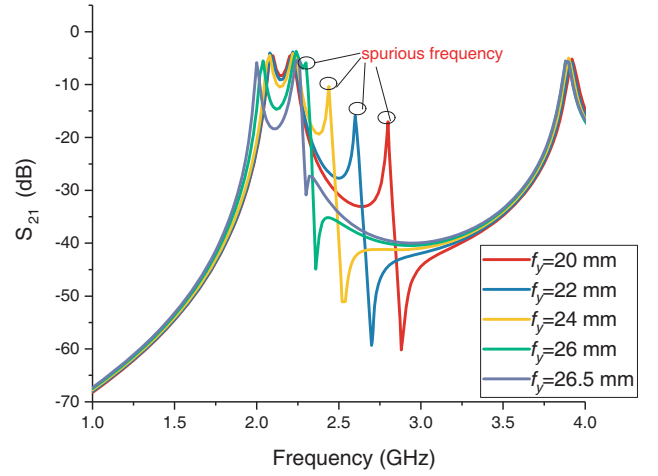


Figure 4. Simulated results versus different f_y .

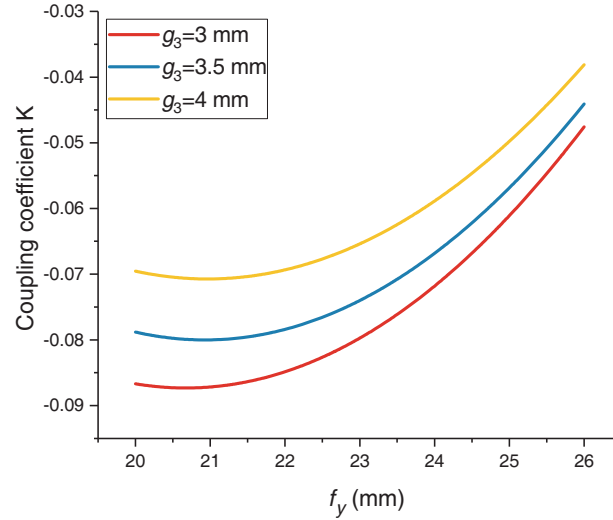


Figure 5. Coupling coefficient K at f_0 against f_y for various iris g_3 .

These two parameters f_y and g_3 may be used to adjust the required coupling coefficient and the slope of curve. Besides, as outlined previously, the required transmission zeros for filter should be adjusted by properly selecting the depth h_f and the combination of f_y and g_3 . All parameters are simulated in electromagnetic simulator ANSYS HFSS.

3. QUARTER-MODE SIW FILTER DESIGN AND EXPERIMENTAL RESULTS

To demonstrate the proposed FDC structure, a fourth-order QMSIW with centre frequency (CF) of 2.15 GHz, fractional bandwidth (FBW) of 13%, and return loss (RL) of 20 dB is designed, simulated, and measured in this section. The structure of inline filter is depicted in Fig. 6(a), which is fabricated on a substrate Rogers 6010 with parameters: $\epsilon_r = 10.2$, $\tan \delta = 0.0023$, and $h = 0.635$ mm. The spacing between metallized via holes with diameter of 0.8 mm is 1.2 mm, which constitutes the edge of the QMSIW cavity.

The inline prototype can be obtained by specific synthesis steps [1, 2], which are presented in Fig. 7. The initial triple sections shown in Fig. 7(a) are obtained by optimizing the transverse prototype. The

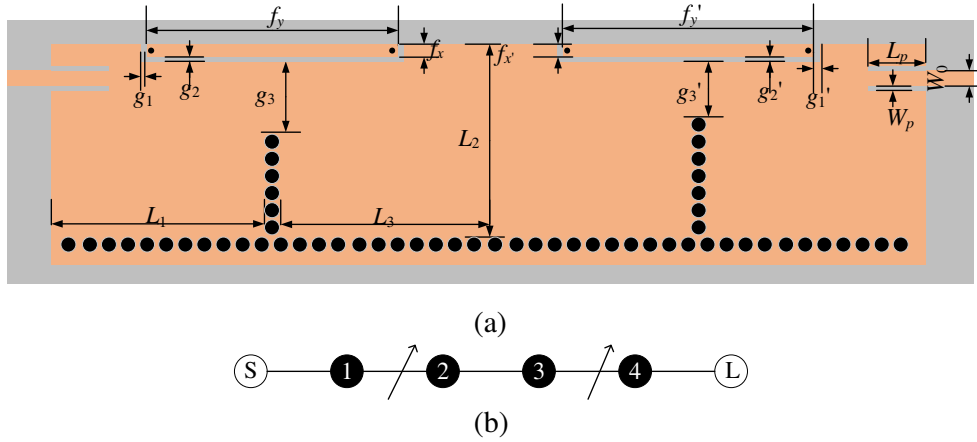


Figure 6. Fourth-order QMSIW filter: (a) the layout of filter; (b) corresponding topology.

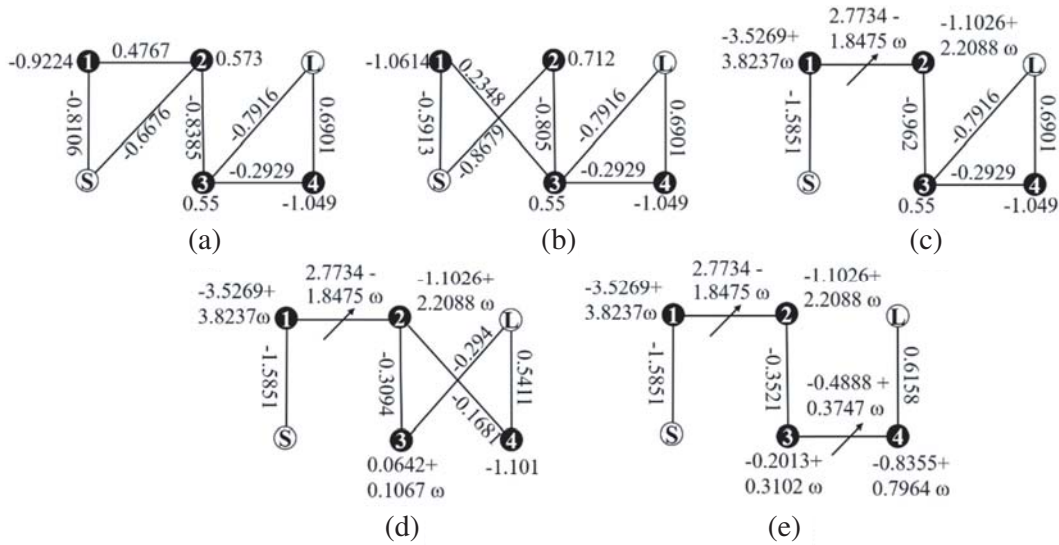


Figure 7. Synthesis procedure of inline filter topology with FDC .

first FDC is detailed in Figs. 7(a)–(c). Similarity transformations are used to obtain the lattice structure as shown in Fig. 6(b). The corresponding admittance matrix A is given by (5), where R is the unity except for the entries $R_{i,i} = R_{j,j} = \cos \theta$, $R_{i,j} = \sin \theta$, $R_{j,i} = -\sin \theta$. θ is the rotation angle defined as follows:

$$A_1 = R_1^T \cdot A_0 \cdot R_1 \tag{5}$$

$$\theta_1 = 0.5 \arctan \frac{2M_{k+1,k+2}}{M_{k+2,k+2} - M_{k+1,k+1}} \tag{6}$$

In order to annihilate the cross couplings between resonators 1 and 3 as well as resonators 2 and source of the lattice network simultaneously, the synthesis continues by successively applying a rescaling transformation on resonator 2 (with rescaling factor α) and another similarity transformation with pivots 1 and 2. U is a diagonal matrix where the main diagonal elements are $U_{k,k} = \sqrt{\alpha_k}$ except for $U_{1,1}$ and $U_{N+2,N+2}$ which equal 1. A new admittance matrix in Eq. (7) is obtained by rescaling transformation on A_1 . A further similarity rotation on A_2 is in Eq. (9), and an inline FDC is ultimately determined, as shown in Fig. 7(c).

$$A_2 = U^T \cdot A_1 \cdot U \tag{7}$$

$$\alpha_k = -\frac{M_{k,k+2} \cdot M_{k+2,k+3}}{M_{k,k+1} \cdot M_{k+1,k+3}} \quad (8)$$

$$A_3 = R_2^T \cdot A_2 \cdot R_2 \quad (9)$$

$$\theta_2 = \arctan \frac{M_{k+1,k+3}}{M_{k+2,k+3}} \quad (10)$$

Afterward, the same matrix manipulations are adopted for another triplet section, where a final in-line topology with two FDCs can be acquired, as depicted in Figs. 7(d)–(e). As a result, frequency-variant coupling matrix (CM) for inline filter is produced in Eq. (11). Fig. 6(b) shows the corresponding inline filter topology, where two FDCs are indicated by a solid line with an arrow. Two TZs are generated by the directly-coupled FDCs in two pairs: one pair is positioned between resonators 1 and 2, while the other is between resonators 3 and 4.

$$\begin{bmatrix} 0 & -0.6864 & 0 & 0 & 0 & 0 \\ -0.6864 & -1.0514 + \omega & -0.9839 + 0.7568\omega & 0 & 0 & 0 \\ 0 & -0.9839 + 0.7568\omega & -0.6524 + \omega & -0.4234 & 0 & 0 \\ 0 & 0 & -0.4234 & -0.4994 + \omega & -0.9543 + 0.6362\omega & 0 \\ 0 & 0 & 0 & -0.9543 + 0.6362\omega & -0.9227 + \omega & 0.8103 \\ 0 & 0 & 0 & 0 & 0.8103 & 0 \end{bmatrix} \quad (11)$$

From the above-mentioned approach, coupling coefficient J_{ij} at centre frequency f_0 should satisfy Eq. (4), and we can also derive the position of TZs. According to Eq. (3), J_{ij} vanishes at a particular frequency: $0.13 \times (-0.9839) + 0.7568(f_{tz}/2.15 - 2.15/f_{tz}) = 0$. Solving this equation yields $f_{tz} = 2.3393$ GHz and a negative root that needs to be discarded. In the same way, the second TZ of 2.3698 GHz can be calculated. Through optimization by HFSS, the ultimate dimensions for filter are: $W_0 = 0.62$, $W_p = 0.1$, $L_p = 4$, $L_1 = 17.6$, $L_2 = 13.13$, $L_3 = 16.6$, $g_1 = g'_1 = 0.2$, $g_2 = g'_2 = 0.3$, $g_3 = 6.3$, $g'_3 = 5.7$, $f_y = 25$, $f_x = 0.6$, $f'_y = 25.58$, $f'_x = 0.4$, unit: millimetres. Considering that the price of buried holes is higher than via holes, the simulated depth of symmetrical metalized holes applied to the physical FDC structure equals the thickness of dielectric plate. Based on the previous discussion, two TZs appear at the upper stopband. The simulation result in Fig. 8 shows that the synthesized transmission zeros are located at 2.33 GHz and 2.36 GHz, which coincides with those computed results.

The comparison of CM, simulated and measured frequency responses are shown in Fig. 8. The proposed filter was fabricated according to the ultimate parameters, and its photograph is inserted in Fig. 8. The measured CF, FBW, RL, and insertion loss are 2.11 GHz, 12.8%, 19.3 dB, and 1.05 dB. The measured responses are almost as expected, except moving down by approximately 45 MHz. Through simulation analysis (which is not given here), we can draw a conclusion that the selected dielectric constant ϵ_r in simulation is 0.2 lower than the one in experiment. Only one FTZ 2.29 GHz can be observed from actual measured curves, which is quite different from the CM. Based on the proposed

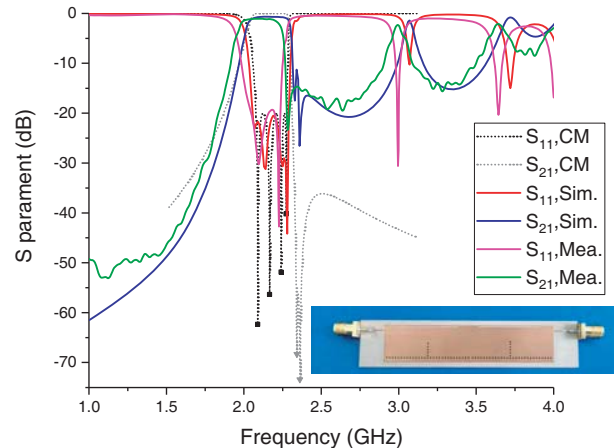


Figure 8. Comparison of frequency response.

fine structure, the same result appears in the simulation analysis. The discrepancy is likely because the via holes or the length microstrip line is larger than the actual designed size. This leads to over-coupling, so phase difference in signal pathway is not 180 degrees, and another TZ disappears.

The performance comparisons between the proposed inline QMSIW filter and previous works are given in Table 1. The proposed filter provides low insertion loss, compact circuit size, and two controllable TZs. Moreover, it is fabricated on the single-layer, which is more convenient to integrate with other circuits.

Table 1. Comparison with previous works.

Ref.	CF (GHz)	FBW (%)	IL (dB)	Topology	TZ NO.	Controllable TZ(s)	Type	Size (λ_g^2)
[4]-I	10.43	3.8	2.34	Inline	1	Yes	SIW	N/A
[5]-III	10	4.35	1.24	Box-section	3	No	SIW	0.94×1.34
[15]	8.45	1.74	0.5	Quadruplet	3	No	QMSIW	1.12×1.39
[17] work-2	8	8.12	0.9	Inline	3	No	Mixed QMSIW & EMSIW	0.43×0.27
[19]	2.4	8.87	2.02	Folded	2	NO	QMSIW	0.24×0.24
This Work	2.15	13	1.05	Inline	2	Yes	QMSIW	0.66×0.14

4. CONCLUSION

In this paper, an inline QMSIW filter with FDCs has been proposed. For the implementation of designed FDC structure, the characteristics and its dimensions corresponding to transmission zeros are analysed. A suitable mix of electrical and magnetic couplings between two adjacent cavities leads to additional TZs which can be controlled by the depth of metalized via holes and the length of the microstrip lines. In order to demonstrate the correctness of the proposed structure, an inline filter with two transmission zeros at the upper stopband has been designed, simulated, and measured. The simulated and measured results show an acceptable agreement and the feasibility of this structure to realize additional controllable transmission zero. It can be seen that FDC can be achieved by means of a suitable mixed coupling, which reduces the number of cross-couplings and simplifies the coupling topology.

REFERENCES

1. He, Y. X., M. Giuseppe, G. Wang, W. T. Wu, L. G. Sun, L. Wang, and R. Zhang, "A direct matrix synthesis for in-line filters with transmission zeros generated by frequency-variant couplings," *IEEE Trans. Microw. Theory Tech.*, Vol. 66, No. 4, 1780–1789, 2018.
2. He, Y. X., M. Giuseppe, Z. W. Ma, L. G. Sun, and Y. Nobuyuki, "Advanced direct synthesis approach for high selectivity in-line topology filters comprising N-1 adjacent frequency-variant couplings," *IEEE Access*, Vol. 7, 41659–41668, 2019.
3. Lukasz, S., L. Natalia, and M. Michal, "A linear phase filter in quadruplet topology with frequency-dependent couplings," *IEEE Microw. Wirel. Compon. Lett.*, Vol. 24, No. 1, 32–34, 2014.
4. Liu, Q., D. F. Zhou, D. W. Zhang, and D. L. Lv, "A novel frequency-dependent coupling with flexibly controllable slope and its applications on substrate-integrated waveguide filters," *IEEE Microw. Wirel. Compon. Lett.*, Vol. 28, No. 11, 993–995, 2018.
5. Liu, Q., D. F. Zhou, D. W. Zhang, and D. L. Lv, "SIW bandpass filters in modified box-section scheme with bypass/constant/frequency-dependent coupling in diagonal cross-coupling path," *IET Microw. Antennas Propag.*, Vol. 13, No. 5, 559–566, 2019.

6. Leszczynska, N., S. Lukasz, and M. Michal, "A novel synthesis technique for microwave bandpass filters with frequency-dependent couplings," *Progress In Electromagnetics Research*, Vol. 137, 35–50, 2013.
7. Gong, K., W. Hong, Y. Zhang, P. Chen, and C. J. You, "Substrate integrated waveguide quasi-elliptic filters with controllable electric and magnetic mixed coupling," *IEEE Trans. Microw. Theory Tech.*, Vol. 60, No. 10, 3071–3078, 2012.
8. Lukasz, S., J. Andrzej, and M. Michal, "A trisection filter design with negative slope of frequency-dependent cross coupling implemented in substrate integrated waveguide (SIW)," *IEEE Microw. Wirel. Compon. Lett.*, Vol. 23, No. 9, 456–458, 2013.
9. Lukasz, S., L. Adam, and M. Michal, "Coupled-resonator waveguide filter in quadruplet topology with frequency-dependent coupling — A design based on coupling matrix," *IEEE Microw. Wirel. Compon. Lett.*, Vol. 22, No. 11, 553–555, 2012.
10. Lukasz, S., L. Natalia, and M. Michal, "Generalized Chebyshev bandpass filters with frequency-dependent couplings based on stubs," *IEEE Trans. Microw. Theory Tech.*, Vol. 61, No. 10, 3601–3612, 2013.
11. Zhu, F., W. Hong, J. X. Chen, and K. Wu, "Quarter-wavelength stepped-impedance resonator filter with mixed electric and magnetic coupling," *IEEE Microw. Wirel. Compon. Lett.*, Vol. 24, No. 2, 90–92, 2014.
12. Amari, S., F. Seyfert, and M. Bekheit, "Theory of coupled resonator microwave bandpass filters of arbitrary bandwidth," *IEEE Trans. Microw. Theory Tech.*, Vol. 58, No. 8, 2188–2203, 2010.
13. Lukasz, S., L. Adam, and M. Michal, "Coupled-resonator filters with frequency-dependent couplings: coupling matrix synthesis," *IEEE Microw. Wirel. Compon. Lett.*, Vol. 22, No. 6, 312–314, 2012.
14. Stefano, M., T. Cristiano, B. Maurizio, and P. Luca, "Quarter-mode cavity filters in substrate integrated waveguide technology," *IEEE Trans. Microw. Theory Tech.*, Vol. 64, No. 8, 2538–2547, 2016.
15. Zhang S., X. D. Fu, J. J. Cheng, D. Q. Cheng, H. T. Wang, F. L. Liu, and L. C. Bao, "Compact balanced bandpass filter with the fractal defected structures," *IEICE Electron. Expr.*, Vol. 15, No. 15, 1–6, 2018.
16. Li, P., H. Chu, and R. S. Chen, "Design of compact bandpass filters using quarter-mode and eighth-mode SIW cavities," *IEEE Trans. Compon. Packaging Manuf. Technol.*, Vol. 7, No. 6, 956–963, 2017.
17. Phirun, K. and J. Yongchae, "Compact and wide stopband substrate integrated waveguide bandpass filter using mixed quarter- and one-Eighth modes cavities," *IEEE Microw. Wirel. Compon. Lett.*, Vol. 30, No. 1, 16–19, 2020.
18. Wang, X., X. W. Zhu, Z. H. Jiang, Z. C. Hao, Y. W. Wu, and W. Hong, "Analysis of eighth-mode substrate-integrated waveguide cavity and flexible filter design," *IEEE Trans. Microw. Theory Tech.*, Vol. 67, No. 7, 1–12, 2019.
19. Liu, Q., D. F. Zhou, D. Zhang, S. Wang, and D. Lv, "Compact cross-coupled quarter-mode SIW bandpass filters with different locations of input and output ports," *2019 International Conference on Microwave and Millimeter Wave Technology (ICMMT)*, 1–3, Guangzhou, China, 2019.